Proceeding of the IEEE
International Conference on Robotics and Biomimetics
Dali, China, December 2019

Pose estimation of components in 3C products based on point cloud registration

Dengwei Dong, Xiansheng Yang, Haopeng Hu and Yunjiang Lou, *Senior Member, IEEE*
School of Mechanical Engineering and Automation
Harbin Institute of Technology, Shenzhen
louyj@hit.edu.cn

***Abstract*— In order to meet the industrial high-precision assembly requirement for components in 3C products, which is texture-less and highly symmetrical, a non-contact pose estimation scheme based on point cloud registration is proposed. The scheme use global registration to quickly find the initial coarse pose of the 3C assembly relative to the camera. Considering the singularity problem caused by the high symmetry of the components in 3C products, template-based algorithm is introduced to eliminate the singular pose, then local registration is used to improve the accuracy of the initial pose based on the global registration result. In order to avoid the local registration algorithm falling into local optimum due to insufficient accuracy of the initial pose, we use improved Globally Optimal Iterative Closest Point (Go-ICP) to performs a finer search in the small space including the global optimal pose. The reliability and effectiveness of the scheme are verified by simulation and experiments.**

***Index Terms*— Model-based registration, Pose singularity, Template-based pose estimation.**

I. Introduction

3C is the abbreviated name of computer, communication and consumer electronics products. With the increase in the production and quality requirements of 3C products on the market, it is of great significance to complete the automated assembly of the 3C production line and to liberate the complicated labor. Pose estimation of components in 3C products is the basis of 3C assembly automation, at present, pose estimation based on point cloud registration is widely used in the field of pose estimation due to the non-contact advantages. For 3C assembly task, high symmetry of the components in 3C products can easily lead to assembly failures, so achieving fast, high-precision, automatical 3C assembly is an important issue.

A simple classification of 3D rigid registration methods can be made based on the type of the underlying optimization method used: global or local [1]. The global registration algorithm can directly estimate the rigid transformation parameters of the two-point cloud without providing an initial pose. The most commonly used global registration algorithms are feature correspondence [2][3][4] and exhaustive search [5][6]. Several feature descriptors such as CVFH, ESF, GRSD, FPFH, RoPS and TriSI are proposed for feature correspondence, In addition, Principal Component Analysis (PCA) is often used in global registration algorithms as a generalized feature. K-D tree, Hash table and Octree are usually used to accelerate the feature match by using the structural information of high-dimensional data. Exhaustive search can obtain the best rigid transformation parameters by traversing the solution space. When the point cloud size is large, the time complexity is high, but the efficiency of the algorithm can be effectively improved by adding constraints. The algorithm based on branch and bound also searches in the whole solution space. By dividing the solution space into different subspaces, the subspaces that are impossible to obtain the global optimal solution are excluded, thereby improving the space search efficiency.

The local registration[7] algorithm iteratively optimizes the euclidean distance of the corresponding point pair of two point cloud based on the initial pose. The precision and efficiency of the micro-adjustment of the local registration algorithm are directly affected by the initial value. If the initial value is high, the iterative optimization can skip the minimum value and convergence to the global optimal solution at a faster speed. Iterative Closest Point(ICP) [8] algorithm and its improved version [9][10] are the most commonly used local registration algorithms, because ICP has a good theorem: for the mean-square distance objective function, ICP can always monotonically converge to a local minimum. Considering the advantages and disadvantages of the two types of algorithms, we use the local registration algorithm to perform a finer search based on the results of global registration.

Pose estimation of components in 3C products existing two main problems: pose ambiguity and iterative registration algorithm falling into local optimum. Pose ambiguity is caused by the low feature and high symmetry of components in 3C products, In this paper, we use the point cloud registration based on PCA decomposition to obtain four sets of poses, and then use template matching algorithm based on LINEMOD feature to eliminate singular poses. The iterative algorithm is trapped into the local optimum due

This work was supported partially by the NSFC-Shenzhen Robotics Basic Research Center Program (No. U1713202) and partially by the Shenzhen Science and Technology Program (No. JCYJ20180508152226630).

Dong, Yang, Hu, Lou (the corresponding author) is with the School of Mechanical Engineering and Automation, Harbin Institute of Technology Shenzhen, HIT Campus, University Town of Shenzhen, Xili, Nanshan, Shenzhen, China. (louyj@hit.edu.cn)

978-1-7281-6321-5/19//$31.00 ©2019 IEEE

to the insufficient accuracy of the initial values provided, therefore we use improved GO-ICP to perform finer search only in the local region obtained by the global registration algorithm, which overcomes the efficiency problem of global GO-ICP.

The remainder of this paper is organized as follows: In Section II, the global registration algorithm based on Principal Components Analysis (PCA) [11][12] decomposition together with template-based LINEMOD [13] is introduced. In Section III, improved GO-ICP [14][15] algorithm is specifically applied to avoid the problem that the local registration algorithm is trapped into a minimum value due to less accurate initial pose. In Section IV, the reliability and feasibility of the whole 3C assembly pose estimation scheme are verified from simulation and experiments.

II. Global registration based on PCA decomposition and LINEMOD

In this chapter, we first introduce the global registration algorithm based on PCA decomposition, and the singular pose problem appeared in the global registration algorithm because of the high symmetry of components in 3C products, then introduced the pose estimation algorithm based on LINEMOD, which is used to filter out the singular poses.

A. Global registration based on PCA decomposition

We use back cover of mobile phone as our assembly target, and the characteristics of the back cover of the mobile phone is used to develop a specific scheme, and hardware of our estimation scheme is shown as figure 1.

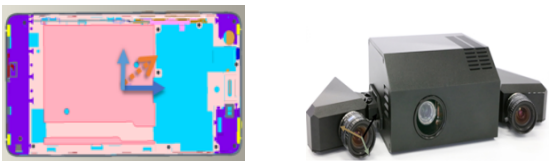

(a) Cell phone back cover (b) Binocular structured light

Fig. 1: Hardware of our estimation scheme

We first get the 3D point cloud through the binocular structure light, and extract the rectangular surface using the Random Sample Consensus (RANSAC) [16] algorithm, then perform PCA decomposition on its covariance matrix. The eigenvectors corresponding to the three eigenvalues form the local coordinate system of the assembly target, and the local coordinate system is basically consistent with the CAD model coordinate, which is set up in off-line phase, so it can be used as the initial pose of the CAD model coordinate system relative to the camera coordinate system. The covariance matrix be calculated by formula as follows

$$J = \frac{1}{n}\sum_{i=1}^{n}\left\{\left(p_i - \frac{1}{n}\sum_{i=1}^{n}p_n\right)\cdot\left(p_i - \frac{1}{n}\sum_{i=1}^{n}p_n\right)^T\right\} \quad (1)$$

The covariance matrix is decomposed by PCA to obtain the feature vector as follows:

$$x = \begin{bmatrix} N_1 \\ N_2 \\ N_3 \end{bmatrix} = \begin{bmatrix} N_{11} & N_{12} & N_{13} \\ N_{21} & N_{22} & N_{23} \\ N_{31} & N_{32} & N_{33} \end{bmatrix} \quad (2)$$

The corresponding eigenvalue decreases. Rotation matrix of point cloud coordinate system relative to camera coordinate system:

$$R = x^T = \begin{bmatrix} N_1 & N_2 & N_3 \end{bmatrix} = \begin{bmatrix} N_{11} & N_{21} & N_{31} \\ N_{12} & N_{22} & N_{32} \\ N_{13} & N_{23} & N_{33} \end{bmatrix} \quad (3)$$

Translation matrix of point cloud coordinate system relative to camera coordinate system can be obtained by calculating the point cloud centroid.

$$T = \begin{bmatrix} t_x \\ t_y \\ t_z \end{bmatrix} = \begin{bmatrix} p_{1x}+p_{2x}+p_{3x} \\ p_{1y}+p_{2y}+p_{3y} \\ p_{1z}+p_{2z}+p_{3z} \end{bmatrix} /n \quad (4)$$

B. Singular pose eliminated by LINEMOD

By analyzing the causes of singular poses, this paper proposes a scheme to filter out singular poses based on the LINEMODE algorithm, which exploits both depth and color images to capture the appearance and 3D shape of the object in a set of templates covering different views of an object. Problems such as efficiency, extra memory requirements and insufficient precision are the reasons why we don't use the algorithm alone for pose estimation. By setting appropriate rendering method and parameters, LINEMODE algorithm can eliminate singular poses to some extent.

1) Causes of singular poses in 3C assembly tasks: The components in 3C products is texture-less and highly symmetrical. For the global registration algorithm based on feature descriptors, the point feature vector of the components in 3C products does not have obvious distinguishing, so there are a lot of mismatches shown as figure 2. For the local registration algorithm, It is difficult to set iteration number and error threshold to eliminate possible singular poses. Ambiguous pose of rectangular surface extracted by RANSAC is shown as figure 3. Considering that it is difficult to eliminate singular poses by simply using point cloud information, we use 2D information combined with 3D point cloud information to eliminate singular poses.

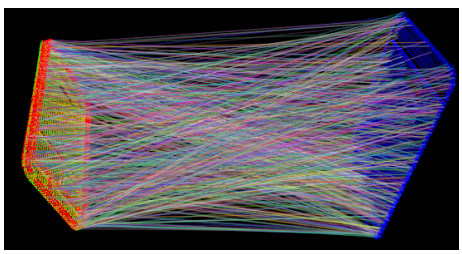

Fig. 2: Mismatches of Fast Point Feature Histogram

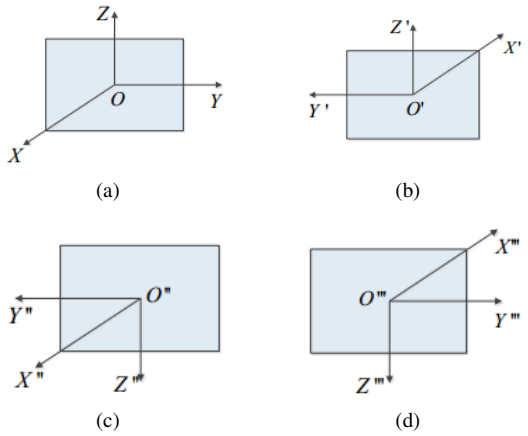

Fig. 3: Ambiguous pose of rectangular surface

2) Theory of template-based LINEMOD: The pose estimation algorithm based on the LINEMOD relies on two different features: the color gradient computed from the color image and the surface normal computed from the object 3D model. In the off-line phase, the rendered color and depth images, captured from different views of the object, are saved as templates, then calculate the LINEMOD feature from these set of templates. In the online stage, match online LINEMOD feature with the off-line LINEMOD feature, and use the pose information of the most similar off-line LINEMOD feature as a reference for filtering out the singular pose.

3) Rendering depth and color images based on CAD models: We render depth and color images from different view of the target covering the entire surface of the object as much as possible while considering the efficiency of the algorithm. The working distance of our binocular structure is 300 mm, but considering working distance deviation and the template is discrete in the three-dimensional space, we generate templates varying from 250-350 mm, using a step size of 10 mm. We use Fibonacci's sampling method to sample on the spherical surface instead of latitude-longitude grid sample method because of the evenly distributed characteristic of sampling points shown as figure 4. The elevation angle of the virtual camera relative to the world coordinate system is set to 60-90° to eliminate extreme view according to our actual assembly requirement.

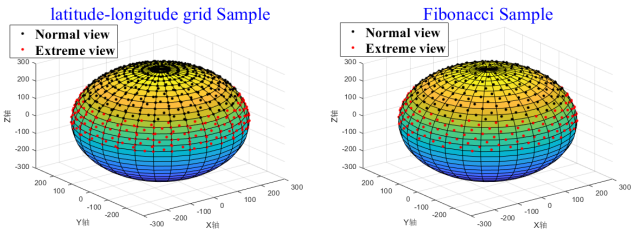

(a) Latitude-longitude grid Sample (b) Fibonacci Sample

Fig. 4: Sample method on spherical surface

4) Strategy to eliminate singular poses: The rigid transformation matrix is decoupled into euler angle vector and translation vector. The multiple solutions obtained by PCA decomposition are compared with the solutions obtained by LINEMDO algorithm. The poses with large difference in euler angle and translation vector are eliminated as singular pose.

III. Local registration algorithm based on improved GO-ICP

In this chapter, we first introduce the ICP and BNB algorithm, then we introduce the improved GO-ICP algorithm to overcome the problem that it may fall into local optimum due to insufficient accuracy of the initial pose.

A. ICP algorithm

Providing a good initial pose, the ICP algorithm can achieve high convergence precision. The formula is as follows:

$$\min_{R,t} E(R,t) = \min_{R,t} e_i(R,t) = \frac{1}{2}\sum_{i=1}^{n} \|p_i - (R \cdot p_i + t)\|^2 \quad (5)$$

Where p_i, q_i are the points from the origin point cloud and the target point cloud respectively. By definition equation 5:

$$\begin{cases} p = \frac{1}{2}\sum_{i=1}^{n} p_i \\ q = \frac{1}{2}\sum_{i=1}^{n} q_i \end{cases} \quad (6)$$

We can convert the formula that needs to be solved into:

$$\begin{cases} \arg\min_{R^*} = \frac{1}{2}\sum_{i=1}^{n} \|p_i - p - (R \cdot q_i - q)\|^2 \\ R^* = p - R \cdot q \end{cases} \quad (7)$$

Where p, q are the centroid of the origin point cloud and the target point cloud. The equation can be solved by Singular Value Decomposition [17] or quaternion based algorithm [18]. By theoretically analyzing the process that ICP algorithm iteratively optimize the rigid transformation parameters, The precision of classic ICP algorithm is improved in three aspects: point selecting, point pair matching and error metric.

Through the theoretical analysis of the classic ICP algorithm, combined with the high efficiency and high precision requirements of the 3C assembly, in the iterative optimization process of the ICP algorithm, we uniformly sample all the points in the normal vector space, match points using normal shooting, use point-to-plane distance as error matric.

B. Branch and bound algorithm

Branch and Bound (BNB) algorithm [19][20] searches through the candidate solution space to find the optimal solution, in this paper, a fine search operation is performed in the vicinity of the initial pose. The initial pose space can be represented by the translation space and the euler angle rotation space. The initial pose is shown in the equation 8.

$$H_0 = \begin{bmatrix} \boldsymbol{r}_0 & \boldsymbol{t}_0 \end{bmatrix} = \begin{bmatrix} \alpha_0 & \beta_0 & \gamma_0 & t_{0x} & t_{0y} & t_{0z} \end{bmatrix} \quad (8)$$

The pose after adding a threshold on the initial pose is used as the candidate space, as shown in the equation 9.

$$H = \begin{bmatrix} \alpha_0 + \varepsilon & \beta_0 + \varepsilon & \gamma_0 + \varepsilon & t_{0x} + \varepsilon_1 & t_{0y} + \varepsilon_1 & t_{0z} + \varepsilon_1 \end{bmatrix} \tag{9}$$

ε is rotation threshold and ε_1 is translation threshold.

After a point in the three-dimensional space is disturbed by the euler angle rotation space and the translation parameter space, the upper and lower bounds of the error of any corresponding point are shown in equation 10.

$$\begin{cases} \bar{e} = e_i\left(R_{t_0}, t_0\right) \\ \underline{e} = \max\left(e_i\left(R_{t_0}, t_0\right) - \left(\gamma_{r_i} + \gamma_t, 0\right)\right) \end{cases} \tag{10}$$

γ_{r_i} represents the uncertainty of the rotation parameter at the data point X_i, and γ_t represents the uncertainty of the translation parameter.

The upper and lower bounds of the error function as equation 5 shown, are respectively the sum of upper and lower bounds of all the points, as is shown in equation 11:

$$\begin{cases} \bar{E} = \sum_{i=1}^{n} \bar{e_i}^2 = \sum_{i=1}^{n} e_i\left(R_{t_0}, t_0\right)^2 \\ \underline{E} = \sum_{i=1}^{n} \underline{e_i}^2 = \sum_{i=1}^{n} \max\left(e_i\left(R_{t_0}, t_0\right) - \left(\gamma_{r_i} + \gamma_t, 0\right)\right)^2 \end{cases} \tag{11}$$

When the lower bounds of a space is greater than the current optimal error, there is no global optimal solution in the space, so the spatial subdivision is no longer performed in the space.

C. Improved GO-ICP algorithm solves the problem of ICP falling into local optimum

Improved GO-ICP proposed by us combine BNB and ICP algorithm for pose estimation. Based on the initial pose obtained by the global registration, the small space containing the global optimal solution is subdivided, the subspace where the optimal pose is impossible to occur is eliminated, and search for optimal pose only in the remaining space. in this paper, the rotating spatial parameters satisfy the requirements of the subject, and the accuracy of the translational spatial parameters is insufficient. Therefore, we subdivide the translation space, then prune and trim to efficiently search for higher precision of the translation space parameters.

The process of alternate optimization of BNB and ICP is shown as figure 5:

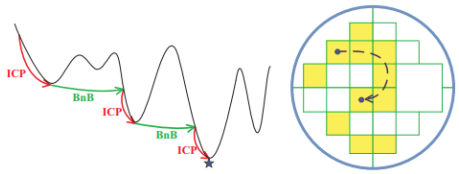

Fig. 5: Alternate optimization of BNB and ICP

IV. Simulation & Experiment

A. Process Design

The process is divided into two parts: simulation and experiment. The program used is written in C++ code. In simulation, point cloud in different view is first rendered, and then use LINEMOD to eliminate the singular poses estimated by the global registration algorithm. We test the ability of LINEMOD for eliminating singular pose experimentally. The eliminate pose is used as the initial value of GO-ICP and the optimal pose is then searched. The pose rendered and calculated is compared in euler angle and translation vector. The only difference between simulation and experiments is whether real-time point cloud, depth and color images are obtained by binocular structured camera. The simulation design process is organized as follows almost the same with experiments design.

Algorithm 1 process design

Definition:
$translation\ \ vector: t_i = \{x,y,z\}, eular\ \ angle\ \ vector: r_i = \{r,p,y\}, Rigid\ \ transformation\ \ matrix\ \ p_i = \{t_i, r_i\}$, linemod feature of template f_i,and its correspondence pose $pf_i, i = 1,2,...,m$, point cloud rendered c_i,and its correspondence pose $pc_i, i = 1,2,...,n$.times of achieving pose requirements of accuracy SP=0.
Algorithm framework flow
for pc_i in pc **do**
  Estimate four Initial inaccuracy pose $pe_j,\ j = 1,2,3,4$ by global pose estimation
  for feature f_i in f **do**
    select the pose pf_k corresponding to most similar template feature f_k with real-time feature
    for j in $1,2,3,4$ **do**
      if $pf_k.r - pe_j.r < \varepsilon_1$ && $pf_k.r - pe_j.r < \varepsilon_2$ **then**
        break
      end if
    end for
    GO-ICP search for final pose PF in area $P = \{pe_j.t + \varepsilon_3, pe_j.r + \varepsilon_4\}$
    if $pc_i.t - PF.t < \varepsilon_5$ && $pc_i.r - PF.r < \varepsilon_6$ **then**
      translation error $t_e = |pc_i.t - PF.t|$,rotation error $r_e = |pc_i.r - PF.r|$
      SP=SP+1;
    end if
  end for
end for
success rate of pose estimate scheme=SP/n;

B. Simulation

1) Ability test of LINEMOD algorithm to eliminate singular pose: We designed three parts of simulation to test its ability of eliminating singular pose.

Simulation 1: Assuming 300mm is the real working distance, we render 500, 750, 1000, 1500, 2000, 2500 templates with different orientation, of which 100 templates are used

as test data, and the remaining is used as training data to test the effect of different number of templates on the accuracy.

TABLE I: Influence of different number of templates on accuracy

Template	Accuracy (%)	Memory (M)	Speed (S)
500	63	2.6	0.067
1000	77	5.8	0.092
1500	90	9.0	0.125
2000	97	12.2	0.144
2500	100	15.4	0.170

Conclusion 1: We have to balance the trade-off between the coverage of the object for reliability and the number of template for efficiency. From this experiment, we need to render more than 2500 templates to get 100% accuracy.

Simulation 2: Assuming we use 300 mm as the working distance to render templates of different orientation, but the actual distance has a deviation of 5 mm, test the effect of different number of templates on the accuracy.

TABLE II: Influence of 5 mm deviation on accuracy

Render Distance(mm)	Working Distance(mm)	Template Number	Accuracy(%)
300	305	2500	93
300	305	3500	96
300	305	5000	98
300	305	7500	100

Conclusion 2: The assumed working distance used to render template deviates from the actual working distance, and the accuracy of 2500 templates now is only 93%, so the number of templates must be increased to achieve higher precision.

Simulation 3: Assuming that there is a greater deviation between the working distance and the actual working distance, test the effect of different number of templates on the accuracy.

TABLE III: Influence of 10 mm deviation on accuracy

Render Distance(mm)	Working Distance(mm)	Template Number	Accuracy(%)
300	310	2500	76
300	310	3500	81
300	310	5000	92
300	310	7500	95
300	310	10000	98

Conclusion 3: When there is a greater deviation between the working distance of the rendering template and the actual working distance, we need to add much more templates to get higher accuracy.

Considering the influence of accuracy, additional external demand, speed and installation deviation of the binocular structure camera, we set the rendering radius varying to 250-350 mm and the rendering step size to 5 mm, the number of rendering templates is set to 5000, the final simulation accuracy is 95%, The result of ICP and Improved GO-ICP is shown as follows:

TABLE IV: Ability of different algorithm for eliminating singular pose

Pose estimation algorithm	Accuracy(%)
SAC-IA	26
FGR	32
GO-ICP	44
scheme proposed by us	95

2) Pose accuracy estimated by ICP and GO-ICP: If the initial pose provided by the global registration algorithm is insufficient, Iterative Closest Point algorithm will easily falling into the local optimal. The GO-ICP algorithm is specifically used to perform fine search in a small area including the global optimal pose to solve that problem. The accuracy of ICP algorithm and the GO-ICP algorithm improved by us is compared by simulation test, the result is shown as figure 6.

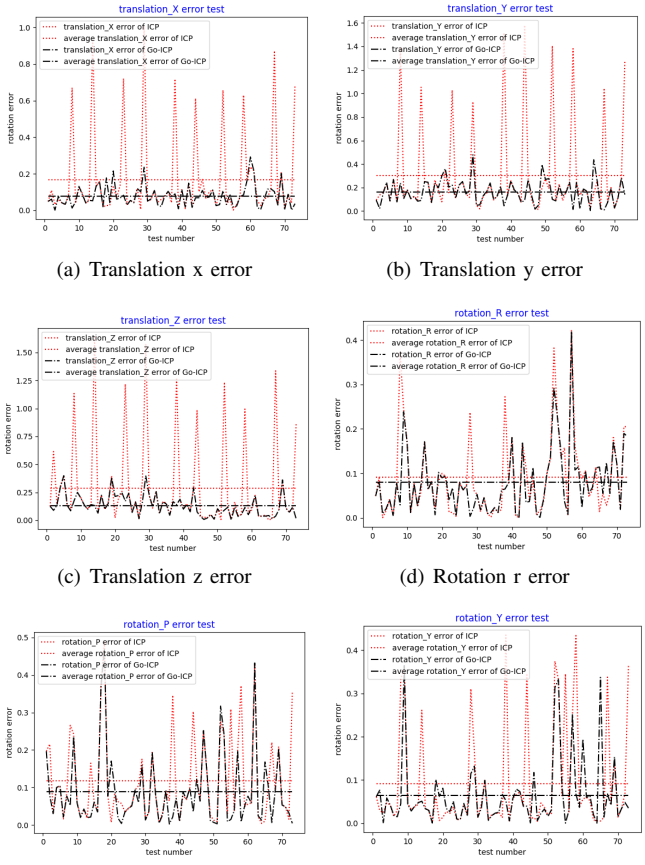

(a) Translation x error (b) Translation y error

(c) Translation z error (d) Rotation r error

(e) Rotation p error (f) Rotation y error

Fig. 6: Comparison between ICP and GO-ICP

Conclusion: The improved GO-ICP algorithm has a large improvement in translation space compared to the ICP algorithm because it prevents the algorithm from falling into local optimum.

3) Stability analysis: We test the robustness of our pose estimation scheme by adding noise to the origin point cloud. Since the accuracy of the binocular structure light is 0.02 mm, gaussian noise with a mean of 0 and a variance of 0.02

mm is added. Robustness test result for noise is shown as table V.

$$\begin{cases} P_{ij}^{noise} = P_{ij} + Z_{ij} \\ Z_{ij} = \left(Z_{ij}^{x}, Z_{ij}^{y}, Z_{ij}^{z}\right) \sim N(\mu, \sum) \\ \sum = E\left[(x-\mu)(x-\mu)^{T}\right] \end{cases} \tag{12}$$

where P_{ij} is point from original point cloud, P_{ij}^{noise} is point from original point cloud adding gaussian noise.

TABLE V: Robustness test for noise

		X Axis	Y Axis	Z Axis
No noise	translation error(mm)	0.08	0.16	0.10
	Z-Y-X Euler angle(°)	0.08	0.09	0.06
Noise added	translation error(mm)	0.088	0.167	0.14
	Z-Y-X Euler angle(°)	0.083	0.094	0.062

From the results, our pose estimation scheme has certain resistance to noise. Because we use the improved go-icp algorithm, even if the accuracy of initial pose provided by our global registration algorithm is rough due to noise, we can still get the global optimal pose to some extent.

C. Experiments

Under the experiments platform we built, the actual test is carried out. We use the pose before and after the UR5 movement as the true pose, which is compared with the pose estimated by our proposed framework on the euler angle vector and the translation vector. The test process is basically the same as the simulation process. The result is as follows:

TABLE VI: Experiment results compared with simulation

		X Axis	Y Axis	Z Axis
Simulation result	translation error(mm)	0.08	0.16	0.10
	Z-Y-X Euler angle(°)	0.08	0.09	0.06
Experiments result	translation error(mm)	0.089	0.172	0.116
	Z-Y-X Euler angle(°)	0.085	0.099	0.067

Since the proposed algorithm itself is robust to noise, the actual experiments accuracy is basically the same as the simulation accuracy. Therefore, the reliability and effectiveness of the scheme proposed by us are verified in simulation and experiments.

V. Conclusion

Through our simulation and experiments, for 3C component, which is texture-less and highly symmetrical, PCA combined with LINEMOD algorithm still can get initial pose of higher precision, and the ability of solving singular pose can achieve accuracy of 95%. The GO-ICP algorithm improved by us avoid falling into local optimum by performing local finer search in a small area including the global optimal pose, and the average accuracy of the whole scheme is improved by about 60% compared with the classic ICP algorithm. The global point cloud registration algorithm proposed in this paper is specifically for components in 3C products with rectangular planes. In the future, We will improve the algorithm to completely eliminate the singular pose, and further improve the efficiency and accuracy.

References

[1] S. Hinterstoisser, S. Holzer, C. Cagniart, S. Ilic, K. Konolige, N. Navab, and V. Lepetit, "Multimodal templates for real-time detection of texture-less objects in heavily cluttered scenes," in *2011 International Conference on Computer Vision*, Nov 2011, pp. 858–865.

[2] J. Yang, H. Li, D. Campbell, and Y. Jia, "Go-icp: A globally optimal solution to 3d icp point-set registration," *IEEE Transactions on Pattern Analysis and Machine Intelligence*, vol. 38, no. 11, pp. 2241–2254, Nov 2016.

[3] J. Yang, H. Li, and Y. Jia, "Go-icp: Solving 3d registration efficiently and globally optimally," in *2013 IEEE International Conference on Computer Vision*, Dec 2013, pp. 1457–1464.

[4] R. B. Rusu, N. Blodow, and M. Beetz, "Fast point feature histograms (fpfh) for 3d registration," in *2009 IEEE International Conference on Robotics and Automation*, May 2009, pp. 3212–3217.

[5] B. Grossmann and V. Krger, "Fast view-based pose estimation of industrial objects in point clouds using a particle filter with an icp-based motion model," in *2017 IEEE 15th International Conference on Industrial Informatics (INDIN)*, July 2017, pp. 331–338.

[6] R. B. Rusu, G. Bradski, R. Thibaux, and J. Hsu, "Fast 3d recognition and pose using the viewpoint feature histogram," in *2010 IEEE/RSJ International Conference on Intelligent Robots and Systems*, Oct 2010, pp. 2155–2162.

[7] A. Aldoma, Z. Marton, F. Tombari, W. Wohlkinger, C. Potthast, B. Zeisl, R. B. Rusu, S. Gedikli, and M. Vincze, "Tutorial: Point cloud library: Three-dimensional object recognition and 6 dof pose estimation," *IEEE Robotics Automation Magazine*, vol. 19, no. 3, pp. 80–91, Sep. 2012.

[8] Byung Cheol Song, Myung Jun Kim, and Jong Beom Ra, "A fast multiresolution feature matching algorithm for exhaustive search in large image databases," *IEEE Transactions on Circuits and Systems for Video Technology*, vol. 11, no. 5, pp. 673–678, May 2001.

[9] M. Gharavi-Alkhansari, "A fast motion estimation algorithm equivalent to exhaustive search," in *2001 IEEE International Conference on Acoustics, Speech, and Signal Processing. Proceedings (Cat. No.01CH37221)*, vol. 2, May 2001, pp. 1201–1204 vol.2.

[10] M. Magnusson, A. Nuchter, C. Lorken, A. J. Lilienthal, and J. Hertzberg, "Evaluation of 3d registration reliability and speed - a comparison of icp and ndt," in *2009 IEEE International Conference on Robotics and Automation*, May 2009, pp. 3907–3912.

[11] P. J. Besl and N. D. McKay, "A method for registration of 3-d shapes," *IEEE Transactions on Pattern Analysis and Machine Intelligence*, vol. 14, no. 2, pp. 239–256, Feb 1992.

[12] S. Rusinkiewicz and M. Levoy, "Efficient variants of the icp algorithm," in *Proceedings Third International Conference on 3-D Digital Imaging and Modeling*, May 2001, pp. 145–152.

[13] D. Chetverikov, D. Svirko, D. Stepanov, and P. Krsek, "The trimmed iterative closest point algorithm," in *Object recognition supported by user interaction for service robots*, vol. 3, Aug 2002, pp. 545–548 vol.3.

[14] J. Fransens and F. Van Reeth, "Hierarchical pca decomposition of point clouds," in *Third International Symposium on 3D Data Processing, Visualization, and Transmission (3DPVT'06)*, June 2006, pp. 591–598.

[15] D. Maatar, R. Fournier, A. Naitali, and Z. Lachiri, "Effect analysis of age and gender on postural stability using pca decomposition," in *2011 IEEE Workshop on Signal Processing Systems (SiPS)*, Oct 2011, pp. 349–354.

[16] Hyun Woo Yoo, Woo Hyun Kim, Jeong Woo Park, Won Hyong Lee, and Myung Jin Chung, "Real-time plane detection based on depth map from kinect," in *IEEE ISR 2013*, Oct 2013, pp. 1–4.

[17] R. M. Haralick, H. Joo, C. Lee, X. Zhuang, V. G. Vaidya, and M. B. Kim, "Pose estimation from corresponding point data," *IEEE Transactions on Systems, Man, and Cybernetics*, vol. 19, no. 6, pp. 1426–1446, Nov 1989.

[18] A. L. D. W. Eggert and R. B. Fisher, "A comparison of four algorithms for estimating 3-d rigid transformations," in *British Conference on Machine Vision*, 1995.

[19] A. Eele and A. Richards, "Rapid updating for path-planning using nonlinear branch-and-bound," in *2010 IEEE International Conference on Robotics and Automation*, May 2010, pp. 3575–3580.

[20] S. Haffner, A. Monticelli, A. Garcia, J. Mantovani, and R. Romero, "Branch and bound algorithm for transmission system expansion planning using a transportation model," *IEE Proceedings - Generation, Transmission and Distribution*, vol. 147, no. 3, pp. 149–156, May 2000.